JGR Space Physics

RESEARCH ARTICLE
10.1029/2021JA029256

The Estimation of D-Region Electron Densities From Trans-Ionospheric Very Low Frequency Signals

E. R. Worthington[1] and **M. B. Cohen**[1]

[1]Georgia Institute of Technology, Atlanta, GA, USA

Key Points:

- D-region electron densities can be estimated from trans-ionospheric Very Low Frequency (VLF) signals.
- A Full-Wave modeling approach can be used to accurately predict trans-ionospheric Very Low Frequency (VLF) propagation.

Correspondence to:

E. R. Worthington,
evan.worthington@gatech.edu

Citation:

Worthington, E. R., & Cohen, M. B. (2021). The estimation of D-region electron densities from trans-ionospheric very low frequency signals. *Journal of Geophysical Research: Space Physics*, *126*, e2021JA029256. https://doi.org/10.1029/2021JA029256

Received 16 MAR 2021
Accepted 25 MAY 2021

Abstract Due to the relatively low ionization levels present in the D-region of the ionosphere (60–90 km), few reliable methods exist for estimating electron densities at this altitude. Very Low Frequency (VLF, 3–30 kHz) radio waves, unlike higher frequency waves used for similar remote sensing applications, are sensitive to these low ionization levels. Much past work has addressed the estimation of D-region electron densities using ground-based measurements of signals originating from VLF transmitters or atmospheric lightning. We introduce a new technique for the estimation of ionospheric D-region electron densities using satellite observations of trans-ionospheric VLF signals originating from high-powered VLF transmitters. Although most of the energy radiated from these transmitters is confined to sub-ionospheric propagation modes, a small fraction penetrates the ionosphere in a right-hand circularly polarized "whistler mode" which has been observed by many satellites. We show that the modal interference pattern previously observed enables the estimation of the electron density profile in the D-region from a single satellite pass. Using data from the DEMETER experiment, each collection is compared with results from a validated theoretical model to select a best-fit D-region electron density profile. Results show expected seasonal variations and are consistent with rocket observations. Although the D-region electron density estimates derived with this technique are shown to exhibit long-term seasonal variations consistent with rocket and ground-based observations, it is important to note that validation of these results remains difficult due to the lack of other techniques for continuously sensing the D-region.

1. Introduction

At Very Low Frequency (VLF, 3–30 kHz), electromagnetic waves can propagate very efficiently over long distances inside of what is often referred to as the Earth-ionosphere waveguide. This region exists between the Earth's surface and the base of the ionosphere. Inside of this region, VLF radio waves are trapped between these two boundaries and form a guided propagation channel that has proven useful for several applications. One prominent example is the US Navy's Fleet Submarine Broadcast System (FSBS) which has been used for decades to provide a near-global communication link to submerged and surface naval vessels. FSBS is composed of several high-power (up to 1 MW) ground-based transmitters distributed around the globe. Another application of terrestrial VLF communication was the passive global positioning system Omega which was ultimately decommissioned in 1997 (Swanson & Tibbals, 1965). A third is in the study of lighting and its associated radio atmospherics (also referred to as sferics) (Cummer et al., 1998). Sferics are the short pulses of VLF energy that are launched by individual strokes of lightning and, like VLF communication links, can propagate long distances and be recorded by VLF receivers. Information from received lightning sferics can be used to determine when and where individual strokes of lightning occur (Said et al., 2010) as well as estimate the state of the lower ionosphere which forms the upper boundary of the Earth-ionosphere waveguide. This region, which is known as the D-region, exists between roughly 60–90 km in altitude. In the daytime, the D-region is primarily the result of ionizing Lyman α and X-ray radiation from the sun. At night, a weaker D-region is sustained by ionization from cosmic rays (Ganguly, 1970; Kockarts, 2002). In addition to the large role it plays in terrestrial VLF communications and in the study of lightning sferics, the ionosphere D-region also plays a large role in the area of trans-ionospheric VLF injection into the magnetosphere (Cohen & Inan, 2012), long-range High Frequency communications (Siskind et al., 2017), and Over-the-Horizon Radar applications (Pederick & Cervera, 2014).

The structure of the D-region plays a crucial role in all the above-mentioned applications. At frequencies below roughly 300 kHz, the D-region essentially forms a reflective layer that represents the upper boundary of the Earth-ionosphere waveguide. At higher frequencies, the D-region primarily acts to absorb

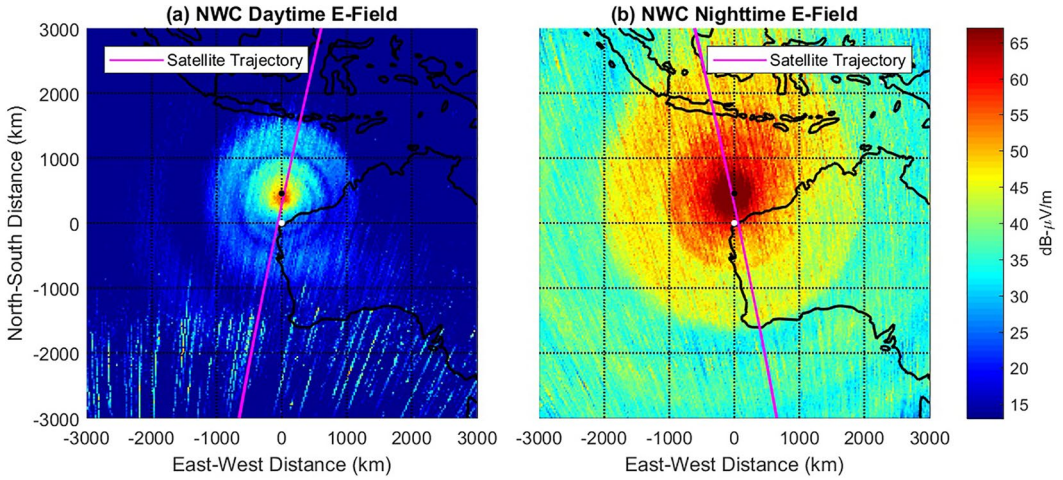

Figure 1. (a) Long-term average daytime electric field as recorded by DEMETER over NWC transmitter. (b) Long-term average nighttime electric field as recorded by DEMETER over NWC transmitter. The white dots in each plot represents the position of the NWC transmitter and the black dots represents the intersection of the magnetic field line that begins at the base of the ionosphere above the NWC transmitter. The magenta lines represent typical trajectories of the DEMETER satellite as it passed overhead of NWC at day and night.

electromagnetic energy through electron collisions with neutral particles (Davies, 1990). Because of its prominent role in so many areas of research, the measurement or estimation of the D-region has been discussed by several researchers (Friedrich & Torkar, 2001; Gupta, 1998; Sechrist Jr., 1975). Unfortunately, for several reasons discussed by Cummer et al. (1998), direct measurements of the D-region electron densities are difficult to obtain and only a small number (∼300) of rocket-based measurements have been recorded (Friedrich & Torkar, 2001). For this reason, several techniques have been proposed to indirectly estimate D-region electron densities using ground-based measurements of lightning sferics (Cummer et al., 1998), FSBS broadcast signals (Gross et al., 2018), or by other means (Higginson-Rollins & Cohen, 2017).

As discussed by Cohen and Inan (2012), a large collection of VLF observations was made by the DEMETER satellite (Parrot, 2002) over a six-year period starting in 2004. Collecting those DEMETER measurements made above each of the FSBS transmitters, an average radiation pattern can be formed under both daytime and nighttime conditions. Furthermore, Cohen et al. (2012) compared the DEMETER measurements with the results from a full-wave method numerical modeling tool (referred to here as FWM) of the type described by Lehtinen and Inan (2008) and found them to be consistent to within a few decibels. Figure 1 shows long-term average electric field measurements as collected by the DEMETER satellite above the NWC transmitter which is located on the western coast of Australia. NWC, like many FSBS transmitters, broadcasts a minimum shift keying (MSK) binary message (Gross & Cohen, 2020), which spreads the spectrum. In the case of NWC, the baud rate is 200 baud (a bit period of 5 ms), which corresponds to a ∼±200 Hz spread spectrum. The NWC signal strength measurements were made by integrating the DEMETER spectral measurements over the bandwidth of the signal.

The signal collected by DEMETER represents a small fraction of VLF energy that transits the ionosphere in a right-hand circularly polarized whistler mode. As discussed by Helliwell (1965), whistler mode waves travel most efficiently along the Earth's magnetic field lines. For this reason, the peak field strength detected by DEMETER occurs roughly 450 km to the north of the NWC transmitter which is marked with a white dot in Figure 1. The precise point where the peak field strength is predicted to occur is found by locating the point in space directly above the transmitter at the base of the ionosphere where the whistler mode wave is formed (70 km) and following the magnetic field lines up through the ionosphere to the DEMETER altitude of 660 km. This point, which is marked with a black dot in Figure 1, shows good agreement with the peak position of the long-term average measurements, although it should be noted that the VLF energy does not precisely follow the geomagnetic field line (Inan & Bell, 1977).

In this work, we present a new technique for estimating D-region electron density profiles by use of measured trans-ionospheric VLF signals originating from FSBS transmitters. First, we discuss several features that are observed in DEMETER collections that occur above the NWC transmitter in Australia (−21.8160 lat, +114.166 lon, 19.8 kHz). Next, we demonstrate that those features vary seasonally as would be expected due to seasonal variations in D-region electron densities. Finally, using the rocket measurements compiled by Friedrich and Torkar (2001), we set bounds on a parametric model for mid-latitude, daytime D-region electron densities and use a numerical modeling tool to simulate the expected seasonal variability of the DEMETER collections and show them to be largely consistent with the measured data.

We suggest that it is possible to estimate D-region electron density profiles using trans-ionospheric VLF signals collected by satellites, even with a single pass. Although we note that the transmitter itself may modify the local ionosphere as has been discussed by several authors (Bell et al., 2011; Inan, 1990), perhaps even by as much as 26% (Rodriguez & Inan, 1994), this effect appears to be small compared to the seasonal and diurnal variations in the D-region or those due to short-term fluctuations in solar activity. We propose how these estimates can be achieved in practice and discuss the viability of this technique in supporting D-region models of varying complexity. The full validation of this estimation technique will require additional satellite measurements that coincide with independent observations of D-region electron densities and could be the subject of further work.

2. Observations

2.1. DEMETER Data

The DEMETER satellite was launched in 2004 to study disturbances in the ionosphere due to seismic activity and anthropogenic sources (Parrot, 2002). It was in almost continuous operation for more than 6 years and followed a quasi sun-synchronous, circular orbit with a high inclination of 98.23°. In 2005, its altitude was changed from 710 to 660 km. Due to its sun-synchronous orbit, DEMETER passed over most points on Earth twice a day, separated by roughly 12 h. At the NWC transmitter, DEMETER would typically make one (north-to-south) daytime pass around 1000 local time and one (south-to-north) nighttime pass around 2200 local time. Because DEMETER recordings in the proximity of the NWC transmitter were limited to one daytime and one nighttime pass each day it was not possible to study the transmitter over a full diurnal cycle. However, because the passes did occur consistently at roughly the same time every day and night, emissions from the transmitter could be explored for seasonal variations which will be discussed below. With the exception of the period between early June 2007 and late January 2008 when the satellite was not recording data, this work included the full six-year DEMETER data set.

The DEMETER satellite employed electric and magnetic field sensors that operated in both a survey (normal) mode and a burst mode which was recorded at a higher data rate above seismically active regions. For this study, survey mode data was exclusively used which provided 20 kHz-wide spectral measurements of the electric and magnetic fields with a frequency resolution of around 20 Hz and a measurement period of 2 s. Signal strength measurements were derived by integrating DEMETER's spectral measurements over the bandwidth of the signal of interest. In the case of the NWC transmitter, the signal was a MSK modulation scheme that occupied a roughly 200 Hz bandwidth centered at 19.8 kHz.

Initially, the full DEMETER data set was down-selected to include only those measurements made within 3,000 km in ground-range of the NWC transmitter. Next, the measurements were organized into individual satellite passes resulting in roughly one daytime and one nighttime pass per twenty-four hour period. Each pass contained a different number of samples depending on how long the satellite's trajectory remained in the 3,000 km window described above. The geographical coordinates (latitude, longitude, and altitude) supplied with each E and H field measurement of the signal were then converted into relative positions along the satellite's trajectory referenced to the point in the trajectory that was closest the transmitter. An example of a satellite pass is shown in red in Figure 2a. After organizing the individual satellite passes, the electric and magnetic field measurements were filtered using a 30th-order, low-pass, FIR filter ($f_{cut} = 3.3 \times 10^{-3}[\mathrm{km}^{-1}]$) to help identify some common features found in most passes. An example of multiple filtered passes are shown in Figure 2b. Finally, upon inspection, it became apparent that a small number of passes (<5%) were anomalous in some way and were removed from the data set. For most anomalous passes, it appeared as if

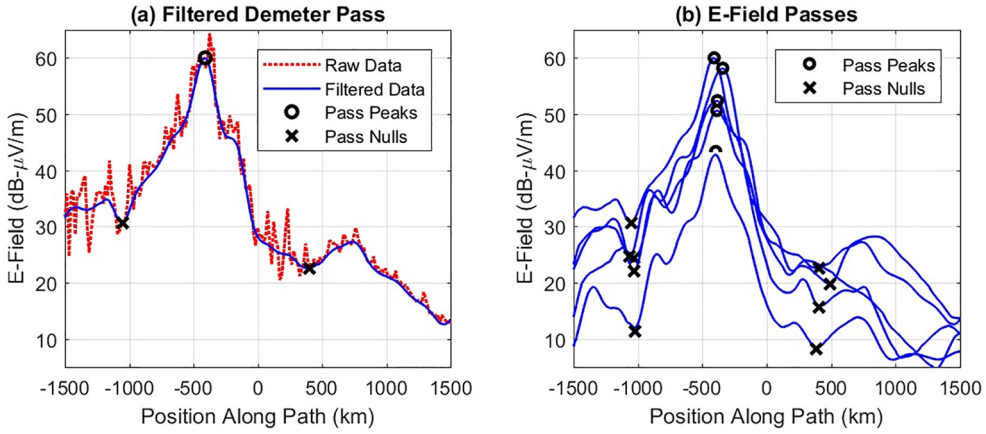

Figure 2. (a) A representative daytime collection from DEMETER as it passed overhead of the NWC transmitter alongside of a filtered version of the same data. (b) Five separate daytime collections (filtered) from a narrow geographical window but recorded at different times of the year. The *x*-axis is referenced to the point on the satellite's trajectory where it is closest to the NWC transmitter. Black circles indicate the position and magnitude of each pass's peak field strength and the black x's indicate the position of each pass's dominant northern and southern null position.

the transmitter was off and no signal was present. For these cases, simply filtering out any pass that did not have a peak E-Field value greater than 30 dB $-\mu$V/m was sufficient.

2.2. DEMETER Pass Features

Several observable features in the daytime electric field measurements made by DEMETER over the NWC transmitter were found to vary seasonally and are consistent with predictions made by numerical modeling tools as D-region electron densities are varied. For most DEMETER collections that passed within 300 km of the NWC transmitter, a very standard electric field pattern was observed. For daytime passes where DEMETER traveled overhead from north-to-south, the pattern consisted of a dominant peak roughly 450 km to the north of the transmitter and strong, predictable local minimums or "nulls" to the north and south of the main peak. Figure 2a shows a typical electric field collection over the NWC transmitter and indicates the dominant peaks and nulls described above.

These peaks and nulls are the result of the unique modal interference pattern created by the VLF transmitter inside the Earth-ionosphere waveguide. These features were persistent and easily identifiable between observations. Figure 2b shows five different DEMETER collections that took place at different times of the year but within a narrow geographical window (represented by the magenta line in Figure 1a). Importantly, the interference pattern is a function of the D-region ionospheric condition.

2.3. Seasonal Variations in DEMETER Data

For each DEMETER collection over the NWC transmitter the amplitude and position of the dominant peaks and nulls were recorded. Seasonal variations were then calculated for these features by first selecting only those DEMETER passes that occurred within a narrow geographical window (specified by a distance to the transmitter and a window width in kilometers). For example, Figure 3a shows the trajectories for all DEMETER collections in a 150 km window centered on the point 85 km to the west of NWC, as indicated by the magenta swath. This subset of DEMETER collections captures the main peak of the transmitter's radiation pattern. Over the lifetime of DEMETER, 71 daytime collections occurred in this window. As can be seen in Figure 3a, collections that occur outside of this window are expected to have very different electric field patterns and would therefore not be directly comparable. Figure 3b shows the electric field data for those 71 daytime passes.

After selecting the DEMETER passes that fell within the window shown in Figure 3a, the features described above were characterized by a seasonal variable. This variable is calculated by Equation 1 and maps the day

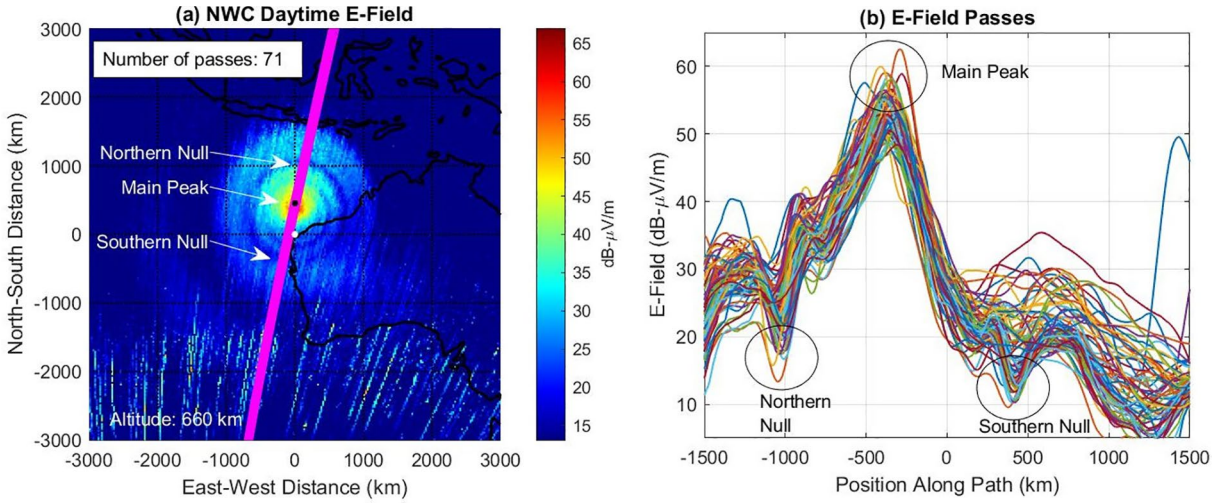

Figure 3. (a) Selection of 71 daytime DEMETER collections that occurred at different times of the year but within a narrow band (magenta lines) of ranges and in close proximity to the NWC transmitter. (b) The electric field measurements (filtered) for the same 71 passes.

of the year (0, 365) to a value on the interval (−1, 1) where −1 is the winter solstice and +1 is the summer solstice in the Southern Hemisphere. In the Northern Hemisphere these values would be reversed. The winter/summer solstice in the Northern/Southern Hemisphere occurs on Dec 21, which is the 355th day of the year which is the reason 355 appears in the numerator of Equation 1.

$$SEASON = cos\left(2\pi\left(\frac{DOY - 355}{365}\right)\right) \tag{1}$$

Figure 4a shows a scatter plot of the peak electric field strength versus season for each of the 71 DEMETER collections discussed above. A linear relationship between peak field strength and season is clearly visible with a Pearson correlation coefficient calculated to be $R = -0.754$ with a p-value of 3.15×10^{-13}, indicating a statistically significant correlation.

The window width of 150 kilometers was chosen to retain a sufficient number of data points while achieving a reasonably homogeneous path geometry across satellite passes. The peak field strengths recorded for this subset of the DEMETER data set vary by roughly 15 dB, (47.6, 62.6 [dB − μV/m]), which aligns closely with simulated results (See Table 1). Figure 4a indicates that about 6.5 dB of this variation is the result of a predictable seasonal change in ionization levels. Figure 4b shows that the peak field strength of the collections falls off at a rate of 0.04 dB/km as the passes are offset from the center of the transmit radiation pattern. Considering a sample window width of 150 km would suggest that roughly 3 dB of variation in the peak field strength may be attributable to the width of the sample window being considered and the fact that each individual satellite pass followed a slightly different trajectory relative to the transmitter radiation pattern (See Figure 4b). This would suggest that the remaining 5.5 dB of variation could be the result of small differences in local solar zenith angle between the measurements and short-term variations in solar activity.

In addition to variations in peak field strength, the position of the northern null was found to vary seasonally as well (See Figure 4c). The position of this null is essentially a measure of the radius of the first prominent ring of energy shown in Figure 3a. The fact that these concentric rings in the transmitter radiation pattern dilate as the height of the ionosphere increases is supported by numerical models and can be seen clearly in Figure 9c and 9d. As with the peak field strength feature, some of the variability in Figure 4c can likely be attributed to the width of the window being considered, however, the overall range of values that this feature takes on is approximately (−1139.6, −985.8 [km]), which is also consistent with simulated results shown in Figure 9d.

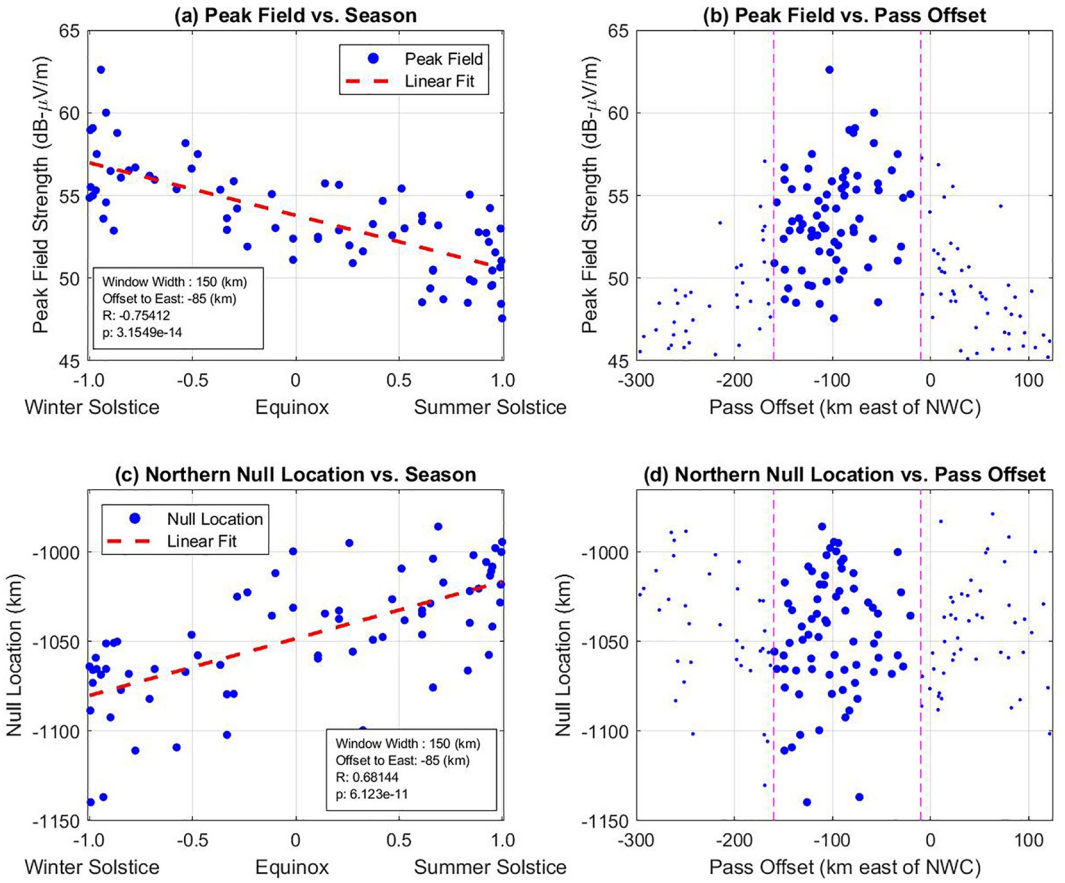

Figure 4. (a) Seasonal variation in peak field strength for the 71 daytime passes described above. (b) Peak field strength versus how far to the East of the NWC transmitter the satellite passed at its closest point. The dashed magenta lines are centered around the 71 collections (heavy-blue dots) that occurred over the peak of the transmit pattern. (c) Seasonal variation in northern null location for the 71 daytime passes described above. (d) Northern null location versus how far to the East of the NWC transmitter the satellite passed at its closest point. The dashed magenta lines are centered around the 71 collections (heavy-blue dots) that occurred over the peak of the transmit pattern.

2.4. Rocket Measurements of D-Region

As discussed by Cummer et al. (1998), there are few reliable methods for measuring the D-region of the ionosphere due to its high altitude and relatively low levels of ionization as compared with the E- and F-regions. A small number of direct rocket measurements of the lower ionosphere, which were collected over a 70-year period, have been gathered and reported on by Friedrich and Torkar (1998) and Friedrich and Torkar (2001).

Considering only those daytime rocket measurements that took place at mid-latitudes (between + /−50°) and which extended down into the D-region (below 80 km) we are left with roughly 100 rocket collections from which we can draw conclusions about the variability that can be expected in the daytime D-region over extended periods. Figure 5 shows the locations of these rocket collections relative to the NWC transmitter as well as the fairly even distribution of these collections over sunspot number (SSN), month, and local solar zenith angle. Because these distributions imply a full range of solar radiation conditions during the rocket collections and because daytime ionospheric electron densities are primarily the result of ionizing solar radiation, we assume that the electron density profiles collected during these rocket experiments approximately

Table 1
Comparison of Observed Versus Simulated Satellite Pass Features

	DEMETER passes	Simulated passes
Min/Max P. Amp. (dB − μV/m)	47.6/62.6	45.9/67.7
Median P. Amp. (dB − μV/m)	53.6	57.2
Δ Peak Amp. (dB)	15.0	21.8
Min/Max Null Position (km)	−1139.6/−985.8	−1106.0/−956.4
Median Null Position (km)	−1046.1	−1030.2
Δ Null Position (km)	153.8	149.8

Abbreviations: Amp, amplitude; P, peak.

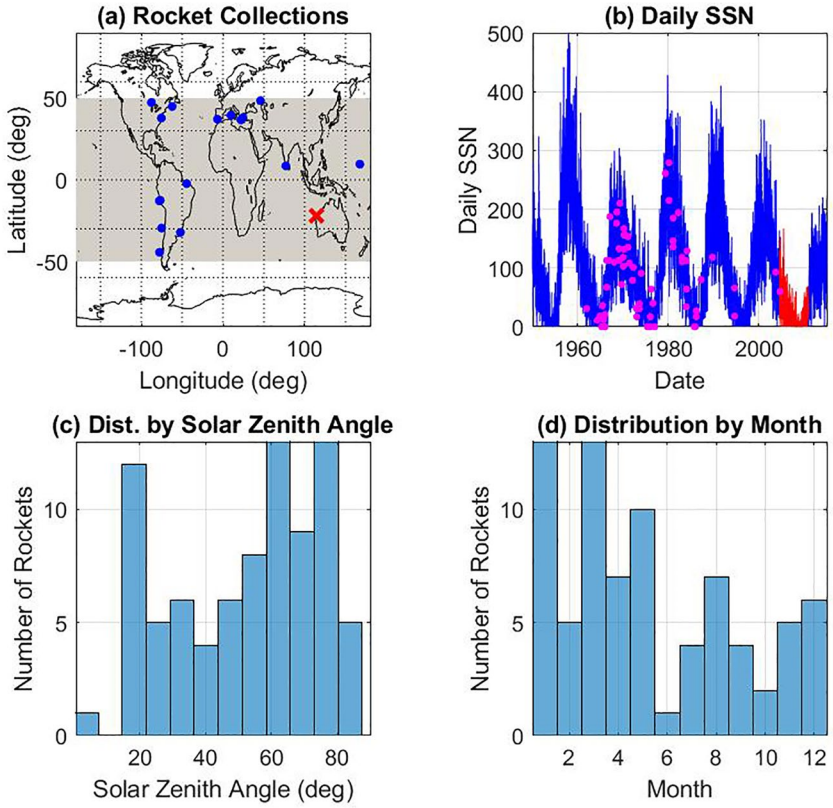

Figure 5. (a) Locations of mid-latitude rocket experiments as compiled by Friedrich. Blue dots represent rocket measurements and the red x marks the location of the NWC transmitter. (b) Plot of daily sunspot number (SSN) overlaid with SSN during rocket experiments (magenta) and SSN during the DEMETER experiment (red). (c) Histogram of the local solar zenith angles during the rocket experiments. (d) Histogram of the months during which the rocket measurements took place.

represent the full range of daytime values that will typically occur over the course of an extended period of time.

Using the rocket experiments described above, Friedrich and Torkar (1998) developed a semi-empirical model of the D-region known as Faraday-International Reference Ionosphere (FIRI) which incorporates variability due to factors such as solar zenith angle, latitude, solar activity, and season into more basic analytical models for D-region electron densities. For this work, the FIRI model was run as an optional setting in the International Reference Ionosphere (IRI) (Bilitza, 2001) which is a widely used empirical model for the mid and upper regions of the ionosphere. Examples of daytime electron densities generated by the FIRI model for mid-latitudes and over a range of solar zenith angles, latitudes, and at different points in the solar cycle are shown in blue in Figure 7a.

Although electron density profiles in the D-region are highly variable as discussed by Budden (1985) and shown directly in Figure 7a, various authors (Cummer et al., 1998; Thomson, 1993) have successfully modeled the D-region using a two-parameter model first described by Wait and Spies (1964). This model, which defines a set of exponential curves, uses two parameters h' and β to set the height and roll-off of the D-region electron density and is represented by Equation 2 where h is the height in kilometers above the earth.

$$N_{em}(h,h',\beta) = 1.43 \times 10^{7} e^{-0.15\,h'} \cdot e^{[(\beta-0.15)(h-h')]} [cm^{-3}] \quad (2)$$

As discussed by Gupta (1998), the D-region of the ionosphere often exhibits a so-called ledge which is a sudden drop or even reversal in the electron density gradient in the region between around 70 and 90 km. The D-region ledge roughly represents the boundary between the ionized nitric oxide of the D-region and the

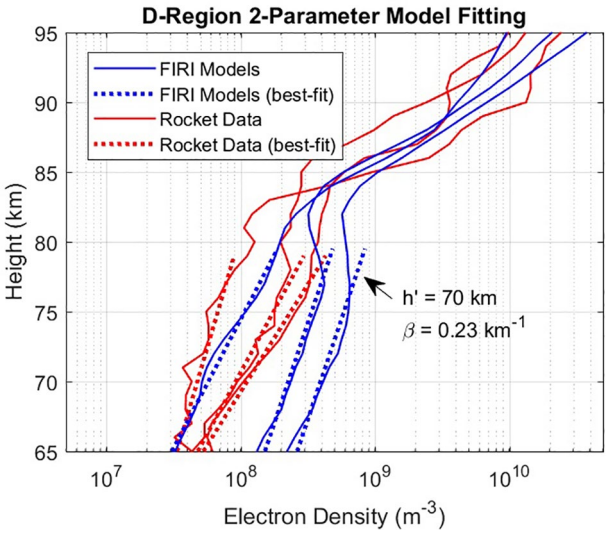

Figure 6. Curve fitting two-parameter D-region models to Faraday-International Reference Ionosphere electron density profiles (blue) and rocket measurements (red).

ionized molecular oxygen of the E-region. Below this ledge the D-region electron density profile typically assumes a more predictable exponential roll-off which is largely captured by the two-parameter model described above. Above the ledge, standardized empirical models such as the IRI have been shown to provide high quality estimates based on data from multiple sources (Bilitza, 2001).

For any given electron density profile (either measured or calculated by FIRI) we can apply a least-squares algorithm to determine the h' and β parameters that best represent that D-region profile between 65 and 80 km. This is done by solving Equation 3 for h' and β where $N_e(h)$ is the curve we're trying to fit and $N_{em}(h, h', \beta)$ is the two-parameter model calculated from Equation 2. For this work, a simple random search algorithm was used to find a minimum for Equation 3 and solve for h' and β.

$$\underset{\substack{h' \epsilon [50,80]km \\ \beta \epsilon [0.15,0.4]km^{-1}}}{argmin} \int_{h=65}^{h=80} \left(\frac{N_e(h) - N_{em}(h,h',\beta)}{N_e(h)} \right)^2 dh \tag{3}$$

Figure 6 shows a few examples of the best fit curves calculated for a handful of electron density profiles. As long as the specified electron density, $N_e(h)$, extends through the region of interest (65–80 km) and is reasonably well-behaved, Equation 3 can be used to determine best fit parameters.

Figure 7a shows the electron density curves (plotted in red) for each of the mid-latitude, daytime rocket collections compiled by (Friedrich & Torkar, 2001) that extend down into the D-region. For each of these curves, the parameter estimation algorithm described above was used to calculate the corresponding set of h' and β values which are plotted with red X's in Figure 7b. As is shown below, greater than 93% of the rocket-based parameter sets fall within the black box plotted in Figure 7b ($h' \epsilon$ [68, 77], $\beta \epsilon$ [0.19, 0.42]). Because of this, we assume that we can reasonably limit h' and β for mid-latitude, daytime D-regions to this domain.

By randomly generating numerous mid-latitude FIRI D-region profiles between 1950 and 2020 and estimating the corresponding h' and β parameters for each one, a collection of example D-region profiles can be assembled that covers the search spaced outlined in black in Figure 7b. These example D-region profiles are plotted (in blue) on top of the rocket collections (red) shown in Figure 7a. The h' and β parameters corresponding to each of these profiles are plotted in Figure 7b along with those of the rocket measurements. Notably, despite thousands of random FIRI electron density profiles being generated, there were significant regions of the search space that do not appear to be supported by the FIRI model and are only sparsely supported by small handful of rocket measurements. For this reason, for subsequent calculations we choose to limit the h' and β parameters to the search space supported by the FIRI model (plotted with blue dots in Figure 7b).

2.5. Full-Wave Model Simulations

Having bounded the behavior of daytime, mid-latitude, D-region electron densities using direct rocket measurements and the FIRI model as described above, we proceed to simulate DEMETER collections above the NWC transmitter over the full range of D-region parameter sets using a full-wave finite element modeling technique. We do this with the dual purpose of (a) demonstrating that the seasonal variation observed in DEMETER peak field strength and null position observations (see Figure 4) can be satisfactorily explained by expected D-region electron density variation, and (b) proposing a forward modeling-based approach for estimating daytime D-region electron density profiles using a satellite collection above a high-powered VLF transmitter.

The full-wave finite element modeling tool used for this work (referred to here as FWM) was derived from code used by Lehtinen and Inan (2008) to model trans-ionospheric VLF electromagnetic radiation from large ground-based transmitters. The code was originally inspired by the work of Wait (1970). Follow-on

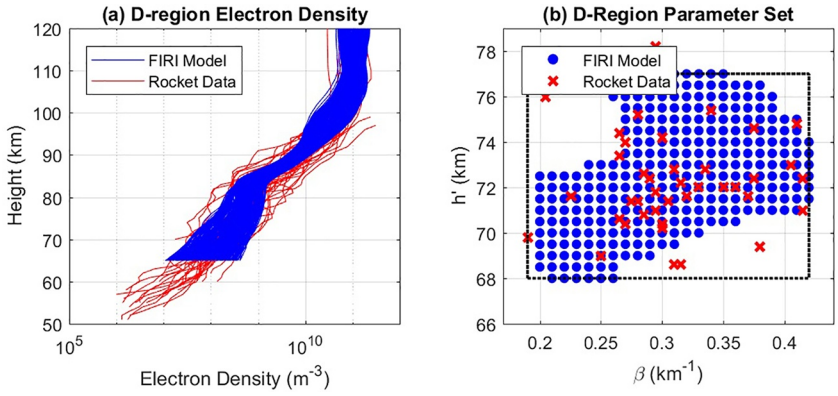

Figure 7. (a) Rocket experiment electron density profiles (red) overlaid with various Faraday-International Reference Ionosphere (FIRI)-generated profiles (blue) that represent the full range of two-parameter sets expected in mid-latitude daytime ionospheres. (b) Estimated values of h' and β parameters for rocket measurements (red) and FIRI-generated profiles (blue). Parameters estimated using best fit technique described above. Black dotted line represents the extent of the search space for the two-parameter model.

work by Lehtinen and Inan (2009) using a limited data set found predictions of satellite-based VLF measurements to be larger than those supported by measured data and postulated that linear mode scattering from irregularities in the ionosphere could explain the discrepancy. Similarly, Starks et al. (2008) examined a number of modeling techniques and also found them to over-predict signal strength when compared with in situ satellite data. Subsequent work by Cohen et al. (2012), however, using a more sophisticated ionospheric model applied to the FWM, and compared to the full DEMETER data set (Cohen & Inan, 2012), found predictions and measurements to be largely consistent.

The relevant parameters required for predicting VLF radio-wave propagation in the D-region are the electron density profile, $N_e(h)$, the electron-neutral collision frequency, $\nu(h)$, and the local geomagnetic field, $\overline{B_0}$. Of these, the electron collision frequency and geomagnetic field are largely static and were assumed to be fixed over time. For this work, the electron-neutral collision frequency was assumed to be that described by Wait and Spies (1964), and is shown in Equation 4 where h is the height in kilometers above the earth. The geomagnetic field was calculated using the International Geomagnetic Reference Field (IGRF) (Finlay et al., 2010) for points above the NWC transmitter during the period of the DEMETER experiment.

$$\nu(h) = 5 \times 10^{11} e^{-0.15(h-70)} \, [s^{-1}] \tag{4}$$

Using the FIRI-generated ionospheres described above, 286 different electron density profiles (represented by blue dots in Figure 7b) were generated that covered the expected range of h' and β parameters seen during the collected rocket experiments. One FWM simulation was completed for each of the 286 FIRI ionospheres. For each simulation, a two-dimensional plot of electric field strength was generated at the altitude of the DEMETER satellite (660 km). From this two-dimensional plot a simulated satellite path can be interpolated that mimics the path taken by DEMETER for the handful of occasions that it passed directly overhead of the NWC transmitter. This simulated satellite collection was then low-pass filtered in the same way as the DEMETER satellite collections described above.

Figure 8 shows a comparison of measurements recorded by DEMETER and a corresponding simulation made using the FWM for the ionosphere defined by $h' = 70.5$ km and $\beta = 0.23$ km^{-1}. As you can see, there is excellent agreement between the measured and simulated results both in terms of the amplitude of the recorded measurements and the position of the peaks and nulls of the recorded data relative to the NWC transmitter which is marked by a white dot. As mentioned previously, the peak field strength recorded by DEMETER occurs ~400 km to the north of the NWC transmitter. This is true because the bulk of the VLF energy that penetrates the ionosphere does so via a whistler mode which propagates roughly along the earth's magnetic field lines.

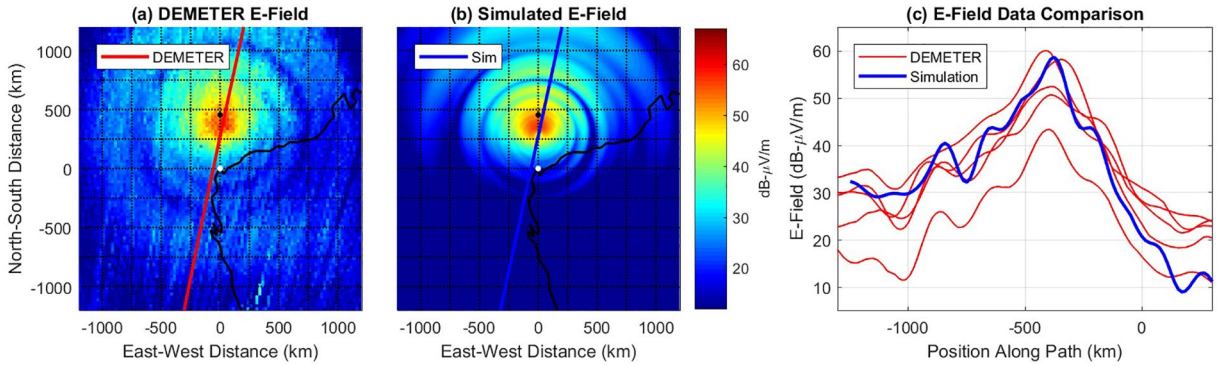

Figure 8. (a) Long-term average daytime electric field as recorded by DEMETER over NWC transmitter. Red lines mark the paths that the DEMETER satellite traveled over five separate collections (closely spaced). (b) Full-Wave Model simulation for a D-region with parameters: $h' = 70.5$ (km), $\beta = 0.23$ (km^{-1}). The blue line represents a simulated satellite pass. (c) Comparison of measured and simulated electric field collections (both low-pass filtered) over the NWC transmitter.

For each of the FWM simulations generated, the peak field strength and the position of the dominant northern null were recorded and are represented in the right-hand panels of Figure 9. As is expected, lower values of h', which correspond to greater ionization in the D-region and hence more attenuation, are associated with lower peak signal strengths. The median peak field strength simulated over the range of ionospheres was 57.2 (dB $-$ μV/m) which is remarkably close to the 53.6 (dB $-$ μV/m) recorded over the DEMETER passes represented in Figures 3 and 4. The range of values calculated for the peak field strength over all available D-region ionospheres was 21.8 dB compared to the 15.0 dB variation seen over the DEMETER collections. The small discrepancy here may have been due to the limited number of DEMETER collections (71) that occurred in this narrow window close to the NWC transmitter. The DEMETER mission took place during a low period of the solar cycle and measurements were not made during periods of high solar activity. Given more satellite collections over a longer period it would not be surprising if that number were to approach the 21.8 dB seen over the simulations.

Similarly, the median null position simulated with FWM occurred at 1030.2 km to the north of the NWC transmitter which is in good agreement with the 1046.1 km median null position recorded by DEMETER. Also very promising is the strong agreement in the total variation of this northern null position. Over the 71 DEMETER collections discussed above, the position of this northern null only varied by 153.8 km which is very close to the 149.8 km variation simulated with FWM over the 286 FIRI ionospheres.

One important result shown in Figure 9 is that while the peak amplitude feature depends primarily on the parameter h' (top-right), the null position feature appears to also have some dependence on the β parameter as well (bottom-right). This should prove valuable if these two features are to be used to infer the D-region electron density parameters h' and β. The positions of other prominent nulls also appear to maintain a similar relationship with the parameter β.

2.6. Estimating D-Region Parameters

A full comparison of the pass features for the DEMETER collections and FWM simulations is collected in Table 1 and offers strong evidence that not only can satellite-based measurements of VLF signals from ground-based transmitters be accurately estimated with numerical modeling techniques but that the amplitude and distribution (relative to the transmitter) of the electric field in this region is largely dictated by the electron density profile present in the D-region at the time of the measurement. As mentioned above, the two prominent features seen in both the measured and simulated data collections (the peak amplitude and northern null position) have been shown to be related to the D-region electron density parameters h' and β. What's more, although the peak amplitude and northern null position features are not fully independent of one another, they do appear to contain different information about the h' and β parameters. It is for these reasons that the authors believe it should be possible to indirectly estimate the D-region parameters h' and

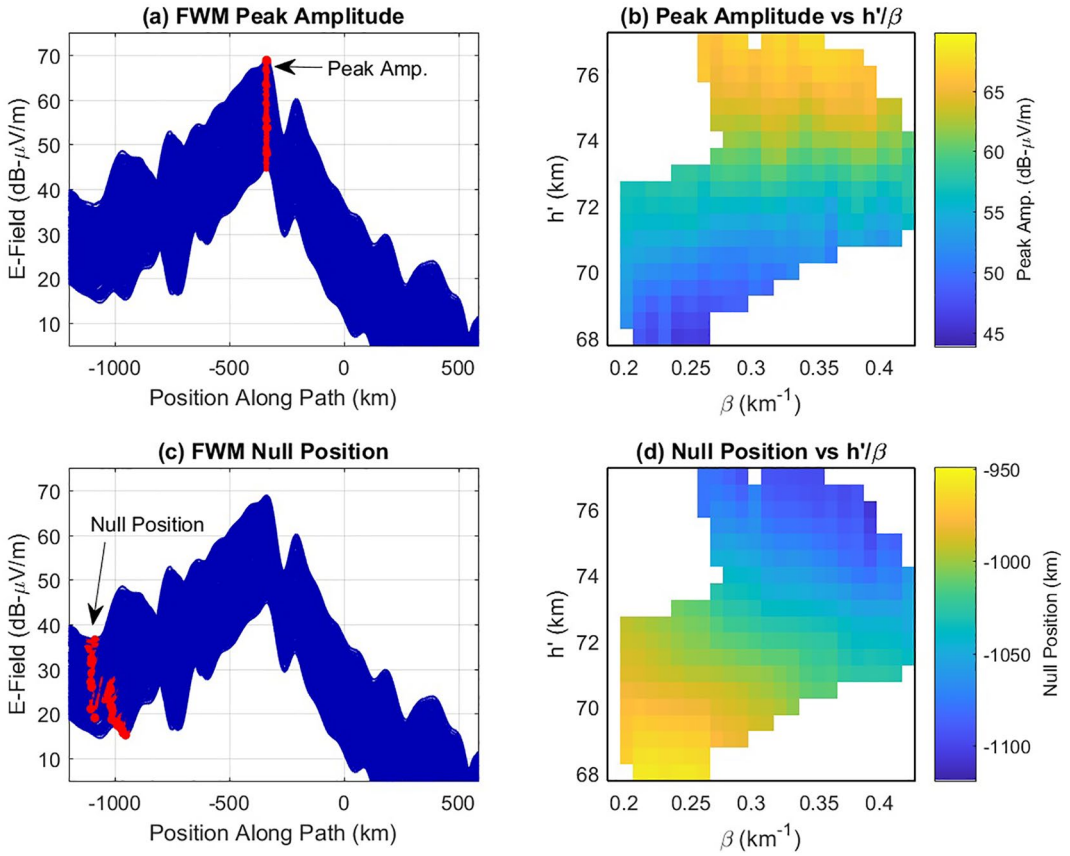

Figure 9. (a) Full-Wave Model (FWM) simulated satellite collections using 286 Faraday-International Reference Ionosphere (FIRI) D-region profiles. Peak amplitude of passes is highlighted in red. (b) Peak amplitudes for simulated passes mapped to each pair of D-region parameters. (c) FWM simulated collections using 286 FIRI D-region profiles. Northern null position is highlighted in red. (d) Northern null position for simulated passes mapped to each pair of D-region parameters.

β, at least above a VLF transmitter, given an observation of the peak amplitude and northern null position of a satellite-based measurement.

Using a numerical modeling tool, such as FWM, to effectively act as a transfer function between a range of D-region electron density parameters and various observable features in the resulting electric field measurements allows us to estimate the structure of the ionosphere's D-region in the vicinity of ground-based VLF transmitters during future satellite collections. As an example, by considering a measurement taken by the DEMETER satellite on March 7, 2006 (shown below in Figure 10a) above the NWC transmitter, the peak amplitude and northern null position can be easily identified after appropriate filtering. Next, a normalized L2 norm can be calculated for these two features between the DEMETER observation and each of the 286 sets of values simulated using the FIRI-generated ionospheres. The result of this L2 norm calculation is shown in Figure 10b and the minimum value (in this case $h' = 70.5$ km, $\beta = 0.30$ km^{-1}) can be interpreted as the most likely set of D-region parameters to lead to such an observation.

The particular features described in this paper and used in the example above (peak amplitude and northern null position) are, of course, only useful for satellite observations that occur within a relatively narrow geographical area close to the NWC transmitter and passing through the peak of the transmitter's radiated pattern (see Figure 8a). For satellite observations that occur outside of this narrow window the observed E-field pattern will look very different from Figure 10a with multiple peaks and nulls occurring at different positions along the satellite's path. In these cases, for any given satellite path, different features may need to be identified and compared to simulated values to produce the desired estimates of h' and β parameters. In most of these cases, however, the desired features will likely need to be related to the overall signal

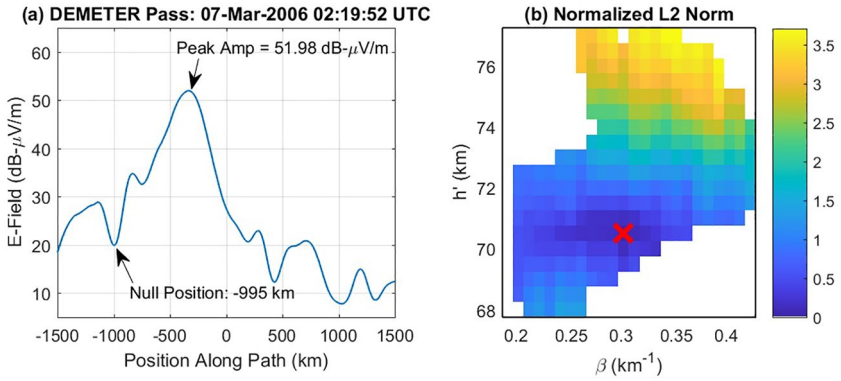

Figure 10. (a) DEMETER collection (filtered) that took place on March 7, 2006. Peak amplitude and northern null position are identified for parameter estimation. (b) Normalized L2 norm calculated over a range of D-region parameter sets. The red "x" marks the minimum of the L2 norm and the estimated value of h' and β.

amplitude and the relative positions of the relevant peaks and nulls in the E-field pattern as these are directly tied to the VLF signal's attenuation as it travels through the D-region and the dominant reflection point of the VLF signal at the base of the ionosphere.

3. Summary

The D-region of the ionosphere plays a crucial role in terrestrial VLF radio wave propagation and a number of other important applications. However, due to several factors, very few direct measurements of ionization levels in this region are available leaving researchers to rely on physics-based models, indirect measurements, and a small handful of direct measurements when performing propagation predictions. Various techniques have been proposed to remotely sense electron densities in the D-region either with ground-to-ground VLF transmission links or through analysis of received lightening sferics by a collection of VLF receivers. The current work introduces a new method of estimating D-region electron densities using trans-ionospheric VLF signals originating from high-powered ground-based transmitters.

Leveraging many years of data collected by the DEMETER satellite, hundreds of electric field measurements made above the NWC transmitter were analyzed and shown to produce a unique modal interference pattern above the transmitter. Considering only those DEMETER collections that passed through the peak of the transmitted radiation pattern, various features were identified across most of the collections and were shown to vary seasonally in a predictable fashion.

Assuming a parameterized model of the ionosphere's D-region which has been used by several authors, a small number of direct rocket measurements were used along with the FIRI model developed by Friedrich to bound the seasonal variation expected in mid-latitude, daytime D-region electron densities. Within this range of D-region parameters, a collection of ionospheres was assembled and used to feed a full-wave, finite element simulation tool which was developed to simulate trans-ionospheric VLF propagation. Results from this simulation tool were found to be highly consistent with DEMETER observations, displaying a seasonal variation nearly equivalent to that observed by the satellite.

For each of the simulated collections, the same features observed in the DEMETER data were labeled and compared against the D-region parameters used to generate each individual simulation. As expected, the observed features were found to vary with the D-region ionospheric parameters being modeled. Finally, it was shown how future satellite-based electric field measurements could be used to estimate D-region electron densities by calculating the normalized L2 norm between the observed features and those simulated over a range of D-region parameter sets. It is important to note that although the distribution of features found in the simulated collections did align quite well with the distribution of the same features found in the DEMETER data (see Table 1), it is currently not clear how accurately any particular set of D-region parameters derived with this method would describe the actual D-region electron density profile in the vicinity of the collection. To achieve this level of validation would require satellite observations of the

trans-ionospheric VLF signal (similar to DEMETER) alongside simultaneous measurements of the D-region electron density profile by direct rocket measurement or other means in close proximity to the VLF transmitter. Although an appropriate data set may be potentially difficult to obtain, this type of technique validation could be the subject of future work.

Finally, as has been discussed by other authors (Bell et al., 2011; Inan, 1990), high-powered VLF transmitter are known to modify the local ionosphere, perhaps by as much as 26% (Rodriguez & Inan, 1994). One potential strength of the proposed estimation technique is that it would provide a measurement of this modified ionosphere. However, a 26% change in D-region electron density is relatively small compared with the seasonal and diurnal variations in this region or others caused by short-term fluctuations in solar activity and would likely not be perceived. For example, using the methods described by Wait and Spies (1964), a 26% change in electron density applied uniformly across the D-region would only result in a change to h' of around 0.77 km. A brief analysis looking at the relative field strengths recorded directly above the transmitter as compared with those further away showed no significant difference between measured and simulated results which assumed a horizontally uniform ionosphere. This indicates that the modification wasn't present or that it simply was not large enough to be perceived by this technique. Ultimately, these estimates are influenced by the seasonal variations discussed above, short-term solar fluctuations, and any ionospheric modifications caused by the transmitter. Separating these effects could require additional ground-based measurements taken further away from the transmitter and a more mature estimation algorithm. Development of these data sets and estimation techniques could also be the subject of future research.

Data Availability Statement

Electric and Magnetic field spectral measurements from the DEMETER mission can be found on the CNES website. http://cdpp.irap.omp.eu/index.php/available-data-cnes.

Acknowledgments
The authors would like to thank Martin Friedrich for his compilation of ionospheric rocket experiments, Nikolei Lehtinen for the use of the FWM model, the IAGA and URSI/COSPAR for their work developing and maintaining the IGRF and IRI models, as well as CNES for access to the DEMETER data set.

References

Bell, T. F., Graf, K., Inan, U. S., Piddyachiy, D., & Parrot, M. (2011). Demeter observations of ionospheric heating by powerful VLF transmitters. *Geophysical Research Letters*, *38*(11), L11103. https://doi.org/10.1029/2011GL047503

Bilitza, D. (2001). International reference ionosphere 2000. *Radio Science*, *36*(2), 261–275. https://doi.org/10.1029/2000rs002432

Budden, K. G. (1985). *The propagation of radio waves: The theory of radio waves of low power in the ionosphere and magnetosphere*. New York: Cambridge University Press.

Cohen, M. B., & Inan, U. S. (2012). Terrestrial VLF transmitter injection into the magnetosphere. *Journal of Geophysical Research*, *117*(A8), A08310. https://doi.org/10.1029/2012JA017992

Cohen, M. B., Lehtinen, N. G., & Inan, U. S. (2012). Models of ionospheric VLF absorption of powerful ground based transmitters. *Geophysical Research Letters*, *39*(24), L24101. https://doi.org/10.1029/2012GL054437

Cummer, S. A., Inan, U. S., & Bell, T. F. (1998). Ionospheric D region remote sensing using VLF radio atmospherics. *Radio Science*, *33*(6), 1781–1792. https://doi.org/10.1029/98RS02381

Davies, K. (1990). *Ionospheric radio*. London: Peter Peregrinus Ltd.

Finlay, C. C., Maus, S., Beggan, C. D., Bondar, T. N., Chambodut, A., Chernova, T. A., et al. (2010). International Geomagnetic Reference Field: The eleventh generation. *Geophysical Journal International*, *183*(3), 1216–1230. https://doi.org/10.1111/j.1365-246X.2010.04804.x

Friedrich, M., & Torkar, K. M. (1998). Empirical D-region modelling, a progress report. *Advances in Space Research*, *22*(6), 757–766. (IRI 1997 Symposium: New Developments in Ionospheric Modelling and Prediction). https://doi.org/10.1016/S0273-1177(98)00095-7

Friedrich, M., & Torkar, K. M. (2001). FIRI: A semiempirical model of the lower ionosphere. *Journal of Geophysical Research*, *106*(A10), 21409–21418. https://doi.org/10.1029/2001JA900070

Ganguly, S. (1970). Role of short-wavelength X rays in the D region ionization. *Journal of Geophysical Research*, *75*(28), 5626–5630. https://doi.org/10.1029/ja075i028p05626

Gross, N. C., & Cohen, M. B. (2020). VLF remote sensing of the D region ionosphere using neural networks. *Journal of Geophysical Research: Space Physics*, *125*(1), e2019JA027135. https://doi.org/10.1029/2019JA027135

Gross, N. C., Cohen, M. B., Said, R. K., & Gokowski, M. (2018). Polarization of narrowband VLF transmitter signals as an ionospheric diagnostic. *Journal of Geophysical Research: Space Physics*, *123*(1), 901–917. https://doi.org/10.1002/2017JA024907

Gupta, S. P. (1998). Diurnal and seasonal variation of D-region electron density at low latitude. *Advances in Space Research*, *21*(6), 875–881. (Proceedings of the C0.1 Symposium of COSPAR Scientific Commission C). https://doi.org/10.1016/S0273-1177(97)00646-7

Helliwell, R. A. (1965). *Whistlers and related ionospheric phenomena*. Mineola: Dover Publications, Inc.

Higginson-Rollins, M., & Cohen, M. (2017). Exploiting LF/MF signals of opportunity for lower ionospheric remote sensing. *Geophysical Research Letters*, *44*(16), 8665–8671. https://doi.org/10.1002/2017GL074236

Inan, U. S. (1990). VLF heating of the lower ionosphere. *Geophysical Research Letters*, *17*(6), 729–732. https://doi.org/10.1029/GL017i006p00729

Inan, U. S., & Bell, T. F. (1977). The plasmapause as a VLF wave guide. *Journal of Geophysical Research*, *82*(19), 2819–2827. https://doi.org/10.1029/JA082i019p02819

Kockarts, G. (2002). Aeronomy, a 20th century emergent science: The role of solar lyman series. *Annales Geophysicae*, *20*, 585–598. https://doi.org/10.5194/angeo-20-585-2002

Lehtinen, N. G., & Inan, U. S. (2008). Radiation of ELF/VLF waves by harmonically varying currents into a stratified ionosphere with application to radiation by a modulated electrojet. *Journal of Geophysical Research*, *113*(A6), A06301. https://doi.org/10.1029/2007JA012911

Lehtinen, N. G., & Inan, U. S. (2009). Full-wave modeling of transionospheric propagation of VLF waves. *Geophysical Research Letters*, *36*(3), L03104. https://doi.org/10.1029/2008GL036535

Parrot, M. (2002). The micro-satellite demeter. *Journal of Geodynamics*, *33*(4), 535–541. https://doi.org/10.1016/S0264-3707(02)00014-5

Pederick, L. H., & Cervera, M. A. (2014). Semiempirical model for ionospheric absorption based on the NRLMSISE-00 atmospheric model. *Radio Science*, *49*(2), 81–93. https://doi.org/10.1002/2013rs005274

Rodriguez, J. V., & Inan, U. S. (1994). Electron density changes in the nighttime D region due to heating by very-low-frequency transmitters. *Geophysical Research Letters*, *21*(2), 93–96. https://doi.org/10.1029/93GL03007

Said, R. K., Inan, U. S., & Cummins, K. L. (2010). Long-range lightning geolocation using a VLF radio atmospheric waveform bank. *Journal of Geophysical Research*, *115*(D23), D23108. https://doi.org/10.1029/2010JD013863

Sechrist, C. F., Jr. (1975). Ionospheric D and E regions. *Reviews of Geophysics*, *13*(3), 894–900. https://doi.org/10.1029/RG013i003p00894

Siskind, D., Zawdi, K., Sassi, F., & Friedrich, M. (2017). Global modeling of the low and mid latitude ionospheric D and lower E regions and implications for HF radio wave absorption. *Space Weather*, *15*, 115–130. https://doi.org/10.1002/2016sw001546

Starks, M. J., Quinn, R. A., Ginet, G. P., Albert, J. M., Sales, G. S., Reinisch, B. W., & Song, P. (2008). Illumination of the plasmasphere by terrestrial very low frequency transmitters: Model validation. *Journal of Geophysical Research*, *113*(A9), A09320. https://doi.org/10.1029/2008JA013112

Swanson, E. R., & Tibbals, M. L. (1965). The omega navigation system. *NAVIGATION*, *12*(1), 24–35. https://doi.org/10.1002/j.2161-4296.1965.tb01802.x

Thomson, N. R. (1993). Experimental daytime VLF ionospheric parameters. *Journal of Atmospheric and Terrestrial Physics*, *55*(2), 173–184. https://doi.org/10.1016/0021-9169(93)90122-F

Wait, J. R. (1970). *Electromagnetic waves in stratified media*. New York: Pergamon.

Wait, J. R., & Spies, K. P. (1964). *Ionosphere waveguide for VLF radio waves*. Washington, DC: U.S. Department of Commerce, National Bureau of Standards.